Draft version November 27, 2024
Typeset using LaTeX **twocolumn** style in AASTeX631

X-ray Constraints on Wandering Black Holes in Stripped Galaxy Nuclei in the Halo of NGC 5128

Samuel L. Feyan [1], Ryan Urquhart [1], Jay Strader [1], Anil C. Seth [2], David J. Sand [3], Nelson Caldwell [4], Denija Crnojević [5], Antoine Dumont [6], and Karina Voggel [7]

[1] *Center for Data Intensive and Time Domain Astronomy, Department of Physics and Astronomy, Michigan State University, East Lansing, MI 48824, USA*
[2] *Department of Physics and Astronomy, University of Utah 115 South 1400 East, Salt Lake City, UT 84112, USA*
[3] *Steward Observatory, University of Arizona, 933 North Cherry Avenue, Tucson, AZ 85721, USA*
[4] *Center for Astrophysics, Harvard & Smithsonian, 60 Garden Street, Cambridge, MA 02138, USA*
[5] *University of Tampa, 401 West Kennedy Boulevard, Tampa, FL 33606, USA*
[6] *Max Planck Institute for Astronomy, Königstuhl 17, 69117 Heidelberg, Germany*
[7] *Universite de Strasbourg, CNRS, Observatoire astronomique de Strasbourg, UMR 7550, F-67000 Strasbourg, France*

ABSTRACT

A subset of tidally stripped galaxies have dense nuclei that are expected to masquerade as massive globular clusters in the halos of large galaxies. If these nuclei contain massive central black holes, some may accrete gas and become observable as active galactic nuclei. Previous studies have found that candidate stripped nuclei rarely host luminous X-ray sources, but were typically restricted to both the most massive candidate nuclei and the most luminous X-ray sources. Here we use new and archival Chandra and XMM-Newton data to search for X-ray emission in a near-complete sample of massive globular clusters and candidate stripped nuclei in the nearest accessible elliptical galaxy, NGC 5128. This sample has the unique advantage that the candidate stripped nuclei are identified dynamically via elevated mass-to-light ratios. Our central result is that 5/22 ($23 \pm 9\%$) of the candidate stripped nuclei have X-ray sources down to a typical limit of $L_X \sim 5 \times 10^{36}$ erg s^{-1}, a fraction lower than or comparable to that among massive clusters with normal mass-to-light ratios (16/41; $39 \pm 8\%$). Hence we confirm and extend the result that nearly all X-ray sources in stripped nuclei are likely to be X-ray binaries rather than active galactic nuclei. If the candidate stripped nuclei have black holes of typical masses $\sim 2 \times 10^5 M_\odot$ needed to explain their elevated mass-to-light ratios, then they have typical Eddington ratios of $\lesssim 2 \times 10^{-6}$. This suggests that it will be challenging to conduct an accretion census of wandering black holes around even nearby galaxies.

1. INTRODUCTION

A central prediction of hierarchical galaxy formation is the accretion of less massive galaxies by a more massive parent (Somerville & Davé 2015). If the orbit of the accreted galaxy takes it close enough to the center of the parent, it can be tidally stripped, as observed in the Galaxy for dwarfs such as Sagittarius (Ibata et al. 1994). Since most galaxies with stellar masses from 10^8 to $10^{10} M_\odot$ have dense nuclear star clusters with typical masses 10^6–$10^8 M_\odot$ (Neumayer et al. 2020), a straightforward expectation is that massive galaxies should be surrounded by a population of a few to many dense stripped galaxy nuclei (Pfeffer et al. 2014).

The discovery of candidate stripped nuclei—historically called "ultra-compact dwarfs" (UCDs)—bloomed as a subfield with the advent of large spectroscopic surveys of massive elliptical galaxies (Hilker et al. 1999; Drinkwater et al. 2000; Phillipps et al. 2001; Drinkwater et al. 2003), eventually augmented by size-based selection primarily using Hubble Space Telescope imaging (e.g., Haşegan et al. 2005; Evstigneeva et al. 2007; Brodie et al. 2011). These surveys identified UCDs as sources that were more massive and/or larger than typical globular clusters.

Spectacular confirmation of the stripping scenario came via the dynamical detection of a $2 \times 10^7 M_\odot$ supermassive black hole in M60-UCD1 (Seth et al. 2014), one of the densest and most massive ($\gtrsim 10^8 M_\odot$) UCDs known, consistent with being the tidally stripped remnant of a Milky Way-mass galaxy (Strader et al. 2013). A few more UCDs have been subsequently confirmed to also host supermassive black holes (Ahn et al. 2017, 2018; Afanasiev et al. 2018), all in UCDs with stellar

masses $\gtrsim 3 \times 10^7 M_\odot$, far beyond the mass regime of normal globular clusters.

The census of the less massive UCDs, with stellar masses $\lesssim 10^7 M_\odot$, bears on multiple open questions in the assembly of galaxies and supermassive black holes. The stripped nuclei preserve a fossil record of tidally disrupted galaxies, with kinematic and chemical information that is challenging to obtain for more distant galaxies. They are also a promising route to constrain the occupation fraction of supermassive black holes for lower-mass galaxies, which informs seeding scenarios for black hole growth (Volonteri 2010). If the occupation fraction is high in lower-mass galaxies, then the supermassive black hole number density in the local universe could be dominated by stripped nuclei (Voggel et al. 2019), and extreme mass-ratio gravitational wave sources detectable by the Laser Interferometer Space Antenna would be more common.

A challenge in this census is that nuclear star clusters (and hence stripped nuclei) overlap in size and mass with globular clusters, which are far more numerous. A small number of the most massive globular clusters in the Milky Way and M31 have been identified as likely stripped nuclei, and in two cases have been shown to contain central black holes. The M31 globular cluster B023-G078, which has a stellar mass $\sim 6 \times 10^6 M_\odot$, hosts a dynamically-detected $\sim 10^5 M_\odot$ supermassive black hole (Pechetti et al. 2022). ω Cen, the most massive Milky Way cluster ($\sim 3 \times 10^6 M_\odot$), has a recent robust detection of an intermediate-mass black hole $> 8200 M_\odot$ via proper motions of individual fast stars at the cluster center (Häberle et al. 2024).

For galaxies beyond a few Mpc, due to the small angular sizes of the expected black hole spheres of influence, it is difficult or impossible to dynamically confirm black holes in the region of stellar mass overlap between UCDs and globular clusters. This has motivated efforts to search for alternative routes to uncover the presence of central black holes in stripped nuclei.

Perhaps the most popular way to identify black holes in massive star clusters has been to search for multi-wavelength accretion signatures. The serendipitous X-ray detection of a tidal disruption event in a distant UCD provides compelling evidence for a central black hole (Lin et al. 2018, 2020), and the $L_X \gtrsim 10^{40}$ erg s^{-1} source HLX-1 is plausibly a stripped nucleus with a central black hole as well (Soria et al. 2017), but such extreme events are rare. However, given the presence of ambient gas shed from evolving stars, central black holes in stripped nuclei should accrete some of this gas and glow in the radio and X-ray as low-luminosity active galactic nuclei (Maccarone 2004).

Radio continuum searches of massive star clusters in several nearby galaxies have not yet turned up any convincing candidates (Wrobel et al. 2016; Wrobel & Nyland 2020). While X-ray sources have been detected in a number of UCDs, in nearly all cases the X-ray emission can be plausibly explained by low-mass X-ray binaries. Indeed, the occurrence of X-ray sources in UCDs is lower than expected based on extrapolation of trends from lower-mass globular clusters (Dabringhausen et al. 2012; Phillipps et al. 2013; Pandya et al. 2016; Hou & Li 2016), suggesting little or no contribution from central black hole accretion.

Here we take a different tack. Dumont et al. (2022) presented a large high-resolution spectroscopic survey of luminous globular clusters and candidate stripped nuclei in NGC 5128 (Cen A), with a goal of obtaining a complete sample of objects $L_V \gtrsim 5 \times 10^5 L_\odot$ (corresponding to $\sim 8 \times 10^5 M_\odot$) within a projected radius of 150 kpc of the galaxy center. This survey targeted candidates selected by Voggel et al. (2020) and Hughes et al. (2021) using photometry and structural information from both Gaia and ground-based imaging. When combined with reliable archival measurements, this effort resulted in a sample of 65 objects with measured dynamical mass-to-light ratios (M/L_V). The central result of Dumont et al. (2022) was evidence for bimodality in M/L_V, with one subpopulation peaking around ~ 1.3 and the other at ~ 2.7. They argued that a natural explanation for this bimodality is if the high-M/L_V group consists of stripped nuclei with embedded central black holes that make up typically $\sim 10\%$ of the remaining stellar mass of the former nucleus (Mieske et al. 2013). The low-M/L_V group would then be either normal globular clusters or stripped nuclei that either lacked central black holes entirely, or had black holes of too low a mass ($\lesssim 10^5 M_\odot$) to have a detectable impact on the integrated velocity dispersion.

In this paper we analyze new and archival X-ray observations for this sample. This is the first direct comparison of X-ray properties for samples of dense star clusters where the identification of candidate stripped nuclei has been done using dynamical M/L_V information rather than simply stellar mass. In principle, this should be more closely linked to the existence of a central black hole than stellar mass alone. In addition, the closer distance of Cen A (3.8 Mpc) compared to the Virgo or Fornax Clusters means that we are sensitive to lower X-ray luminosities than in most previous work systematically searching for X-ray emission from UCDs.

The paper is organized as follows. In Section 2, we describe our methods and data analysis for both Chandra and XMM-Newton X-ray data. In Section 3, we present

our X-ray luminosity measurements and assess them in the context of the existing M/L_V information. Section 4 contains a discussion and summary of the results.

2. X-RAY OBSERVATIONS AND ANALYSIS

Our paper is focused on the sample of 65 luminous Cen A globular clusters or stripped nuclei with dynamical M/L_V (Dumont et al. 2022), discussed in Section 1.

2.1. *Chandra Data*

The majority of the sample had existing Chandra or XMM-Newton data. For eight of the remaining objects, we obtained new Chandra observations (Proposal 23620148, P.I. Strader), using either ACIS-S (7 ksec exposure time) or ACIS-I (9 ksec exposure time), depending on the spatial distribution of the candidates.

The archival data is heterogeneous and in some cases involves multiple independent datasets covering the same source with a mixture of long and short exposure times. For the sources with the largest number of observations and in turn the longest total exposure time, we stacked all ACIS observations above 30 ksec, as long as they were taken with the same chip (ACIS-S or ACIS-I). For sources with lower exposure time we stacked all observations regardless of exposure time or chip.

For the Chandra ACIS observations, we retrieved the data from the archive and re-processed it using the Chandra Interactive Analysis of Observations (`CIAO`) version 4.16.0 (Fruscione et al. 2006). For each source, we defined circular extraction regions appropriately large to fully contain the source. We then extracted the local background using circular regions that total three times the size of the source region.

For the 16 sources with $\gtrsim 50$ counts, we used the `CIAO` task `SPECEXTRACT` to extract a spectrum, using background and response files for each source and observation. We used XSPEC version 12.14.0h for spectral fitting (Arnaud 1996), using a Tuebingen-Boulder ISM absorption model (Wilms et al. 2000), *tbabs*, and a power-law model. Spectra with counts $\gtrsim 250$ were grouped to at least 15 counts per bin to allow χ^2 statistics to be used. Spectra with less counts were left unbinned and fitted using Cash statistics (Cash 1979). In both cases we performed fits with both N_H free and fixed to the Galactic line of sight contribution (2.4×10^{20} cm^{-2}; HI4PI Collaboration et al. 2016). For sources with too few counts to perform robust spectral fitting, we measure the count rate, and then determine the unabsorbed flux assuming an absorbed power-law with N_H fixed to the galactic line of sight contribution and fixed photon index $\Gamma = 1.7$, a typical value expected for the sources in our sample. For all sources the flux reported is the unabsorbed 1–10 keV flux.

In the case of non-detections, we used upper limits from the Chandra Source Catalog (Evans et al. 2010), using the flux_sens_b value and converting it to 1–10 keV. This was to make the upper limits as deep as possible, allowing stacking of all observations across different chip types. For the handful of new observations that did not yet have upper limits listed in the Chandra Source Catalog, we calculated 2σ upper limits by assuming a three count detection with a zero count background, appropriate for short exposure times at these distant locations in the Cen A halo (Kraft et al. 1991).

Unabsorbed fluxes were converted to luminosities using a distance of 3.82 Mpc to Cen A (Harris et al. 2010). 1–10 keV fluxes and corresponding luminosities for all sources are reported in Table 1. The spectral fit properties of sources with sufficient counts for spectral fitting are given in Table 2. For sources with spectral fits, we use the fluxes from the free-N_H fits in all of the other analysis and plots, but also note that the fluxes are typically consistent within 10%, and none of our conclusions would be changed if instead we used the fixed-N_H fits.

Some of the sources with fits in Table 2 show N_H above that expected for Galactic foreground. In a few cases they sit spatially on the dust lane of Cen A which likely explains the inflated N_H: T17-1511 is a particularly clear example where the inferred N_H of 5×10^{21} cm^{-2} is due to Cen A dust. In other cases, the excess N_H could be due to small-scale less obvious dust, or could be internal to the X-ray source due e.g. to a more edge-on orientation.

2.2. *XMM-Newton Data*

For 7 sources with no or limited ($<$ 10 ksec) Chandra data, not counting the new Chandra observations, we supplement using publicly-available XMM-Newton/EPIC data. We processed the data with the Science Analysis System (`SAS`) version 1.3 (`xmmsas_20230412_1735-21.0.0`). Similar to the Chandra observations, we defined circular regions around sources, and rectangular regions on occasions when sources were near chip gaps. We extracted the background using nearby regions at least three times larger than the source region. We selected single and double events (pattern 0-4 for pn and 0-12 for MOS) with standard flagging criteria `#XMMEA_EP` for pn or `#XMMEA_EM` for MOS, in addition to `FLAG=0`. We extracted individual MOS and pn spectra using standard *xmmselect* tasks, before combing them with *epicspec-combine*. The spectral fitting followed the same procedures as for the Chandra data.

For undetected sources, XMM flux upper limits were obtained from the RapidXMM upper limit server (Ruiz

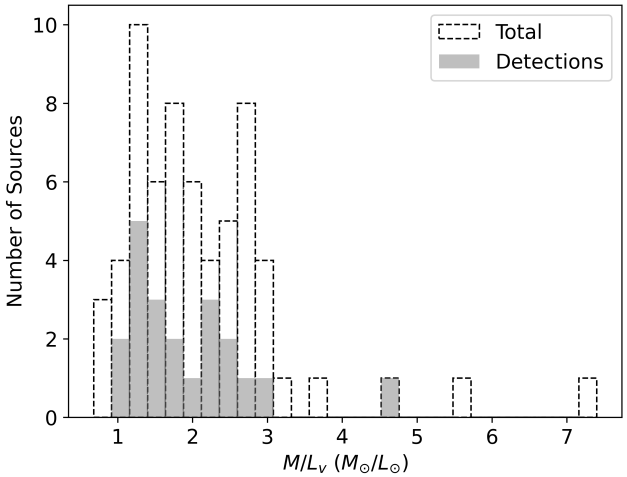

Figure 1. Histogram of M/L_V for all 63 objects (dashed line) and X-ray detections (shaded). The bimodal distribution of M/L_V is visible in both samples.

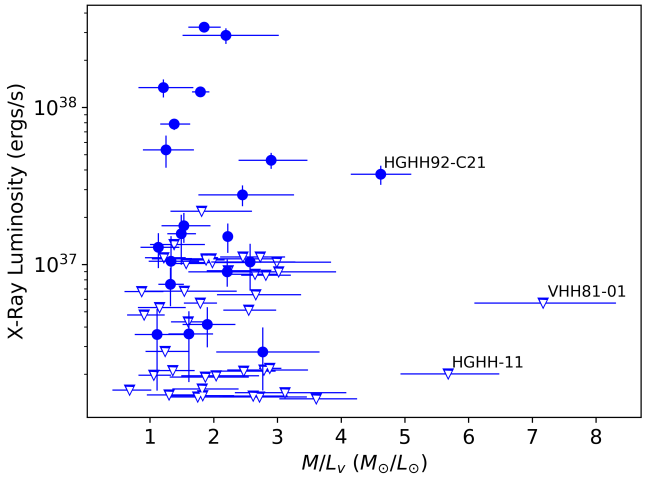

Figure 2. M/L_V vs. 1–10 keV X-ray luminosity for all sources, with detections filled circled and non-detections (upper limits) unfilled downward triangles. The similarities of the X-ray properties of the low and high-M/L_V objects is evident. There are three sources with M/L_V much larger than the other clusters, which have especially strong dynamical cases for being stripped nuclei.

et al. 2022), using the 4XMM catalog (Webb et al. 2020). Wherever data from multiple cameras (MOS1, MOS2, and pn) were available for the same location, we stacked the limiting sensitivities to produce a deeper merged EPIC upper limit.

The results of the XMM analysis are listed in Tables 1 and 2.

2.3. *Final Sample Size*

Of the initial sample of 65 clusters, 63 had an X-ray detection or constraining upper limit from either Chandra or XMM. For the remaining two objects, HGHH-41 fell on a Chandra chip gap, and H12_141 had an XMM slew observation that was too shallow to be useful. These objects are listed at the end of Table 1 for completeness but not included in any subsequent analysis.

We emphasize that most of the 21 X-ray detections have been previously published (Kraft et al. 2001; Minniti et al. 2004; Woodley et al. 2008; Zhang et al. 2011; Pandya et al. 2016), with the exceptions being HH-22, HHH86-34, and HGHH-G251. The central novelty here is the systemic analysis of a dynamically sorted sample of objects.

3. RESULTS

3.1. *M/L_V Subsamples*

The main goal of the study was to compare X-ray properties for the high and low-M/L_V subsamples of the 63 sources with X-ray data. We adopt the Dumont et al. (2022) division of the sample at $M/L_V = 2.3$, which puts 41 sources in the low-M/L_V group and 22 sources in the high-M/L_V group. The number of X-ray detections in the groups are 16/41 ($39 \pm 8\%$) and 5/22 ($23 \pm 9\%$), respectively. The median X-ray upper limit for the non-detected sources is nearly identical for the two groups ($\sim 5 \times 10^{36}$ erg s^{-1}), implying that they are similarly sensitive despite the heterogeneous nature of the sample. The rates of X-ray detection between the subsamples differ only at the 1.5σ level, implying that there is no evidence that the high-M/L_V candidate stripped nuclei host X-ray sources at a rate higher than normal globular clusters. The result is the same if restricted to the more luminous clusters: using only those with $M_V < -10$, 2/13 ($15 \pm 10\%$) of the high-M/L_V group and 8/21 ($38 \pm 11\%$) of the low-M/L_V group are detected in X-rays.

The central result is shown in Figures 1 and 2. Figure 1 shows a histogram of the M/L_V measurements with the X-ray detections shaded, and Figure 2 plots the X-ray luminosity or upper limit against M/L_V. In both figures the similarity of the X-ray properties of the high and low-M/L_V groups are evident.

3.2. *Eddington Ratio Limits for Candidate Stripped Nuclei*

Of the 22 clusters with high M/L_V, 18 have mass estimates for a central black hole from Dumont et al. (2022), and of these 18, 4 have X-ray detections. These were estimated under the assumption that the underlying stellar population has a M/L_V equal to the mean of the low-M/L_V sample ($M/L_V = 1.51$) and then a dynamical model was created for each that added a black

hole of the appropriate mass to reproduce the higher observed M/L_V. While these are necessarily uncertain on an object-by-object basis, and require future high spatial resolution integral field spectroscopy to confirm the dynamical presence of a central black hole, these masses should be on average reasonable if central black holes are the explanation for the elevated M/L_V for these objects. The median inferred central black hole mass is $2 \times 10^5 M_\odot$.

Under these assumptions, we can calculate upper limits to the Eddington fraction—the ratio of the active galactic nucleus bolometric luminosity (L_{bol}) to the Eddington luminosity (L_{edd})—for the putative central black holes in the 14 sources that are *undetected* in the X-rays. To do this, we convert the 1–10 keV X-ray luminosity upper limit to a 2–10 keV limit assuming a power-law with $\Gamma = 1.7$, and then take the bolometric correction measured for low-luminosity active galactic nuclei, $L_{bol} = 15.8\, L_X$ (2–10 keV), from Ho (2009). The resulting Eddington ratio upper limits are listed in Table 1.

The median upper limit is $L_{bol}/L_{edd} < 2 \times 10^{-6}$, with the strongest upper limits about a factor of 3 lower than this. The median *detected* low-luminosity active galactic nucleus in the Ho (2009) sample is somewhat higher, at $L_{bol}/L_{edd} \sim 5 \times 10^{-6}$. Nearly all these galaxies are much more massive than the predicted former host galaxies of the stripped nuclei under consideration here, let alone the stripped nuclei themselves. Nonetheless, it does suggest preliminary evidence that if high-M/L_V stripped nuclei mostly contain central black holes, the Eddington ratio distribution for these sources is different than for low-luminosity active galactic nuclei in more massive galaxies.

3.3. *Interpreting the X-ray Detections*

Because most of the candidate stripped nuclei were not detected in X-ray, the above discussion is largely independent of the interpretation of the 4 detected X-ray sources in these high-M/L_V clusters. Given the lower fraction of X-ray detections among high-M/L_V clusters compared to low-M/L_V clusters, it is a priori plausible that all of these detections are associated with low-mass X-ray binaries rather than with active galactic nuclei. The one exception is HGHH92-C21, which is discussed in more detail below.

3.4. *Individual Objects of Interest*

3.4.1. *HGHH92-C21*

One of the four high-M/L_V sources that is detected in X-rays (mean $L_X \sim 4 \times 10^{37}$ erg s^{-1}) is HGHH92-C21. This cluster has the third-highest M/L_V in our sample (4.6 ± 0.5), far higher than observed for typical globular clusters and consistent with an elevated velocity dispersion due to a central massive black hole. The cluster has a large half-mass radius (~ 9.2 pc) and is very flattened ($\epsilon = 0.33$; Harris et al. 2002), a characteristic shared by nuclear star clusters (e.g., Seth et al. 2006). Voggel et al. (2018) obtained ground-based adaptive-optics assisted integral field spectroscopy to search for a central black hole in HGHH92-C21, but owing to poor data quality were only able to obtain an upper limit of $< 10^6 M_\odot$ on the mass of a black hole.

The X-ray detection of this cluster was previously noted in the Chandra imaging of Kraft et al. (2001). Subsequent work showed that the X-ray source shows frequent short timescale (hundreds of seconds) flares up to $\sim 10^{40}$ erg s^{-1}, a factor of $\sim$ 200–300 higher than its mean luminosity (Irwin et al. 2016). While a stellar-mass compact object cannot be definitively excluded as the source of these luminous flares, the X-ray luminosities and flare timescales would be easily accomodated by a $\lesssim 10^6 M_\odot$ central black hole. HGHH92-C21 is therefore the object in our sample in which the X-ray emission is most likely to have an origin in an active galactic nucleus. Radio continuum imaging to further test this interpretation would be valuable.

3.4.2. *VHH81-01 and HGHH-11*

VHH81-01 and HGHH-11 stand out as having the highest M/L_V in our sample: 7.2 ± 1.1 and 5.7 ± 0.8, respectively, making them strong candidate stripped nuclei with central black holes. This is especially true for VHH81-01 which has a remarkably large half-mass radius of 31.5 pc (Dumont et al. 2022).

Neither is X-ray detected. Despite the relatively shallow XMM data available for VHH81-01, because of its high inferred black hole mass ($8.6^{+10.3}_{-0.1} \times 10^5 M_\odot$; Dumont et al. 2022), the Eddington fraction is the lowest of any cluster in our sample at $< 6 \times 10^{-7}$. Deeper data is plausible, which could allow even tighter constraints on the Eddington fraction of the central black hole likely present.

4. DISCUSSION AND CONCLUSIONS

Our main finding is that luminous star clusters in Cen A that show dynamical evidence for hosting a massive central black hole—likely because most are stripped nuclei—show no enhancement of X-ray sources compared to a control sample of luminous clusters. This result is the straightforward one expected from an extrapolation of previous work, which found that candidate stripped nuclei host X-ray sources at a rate at most comparable to, and usually lower than, other massive

globular clusters (Dabringhausen et al. 2012; Phillipps et al. 2013; Pandya et al. 2016).

There are two ways in which our new result is consistent with but has broader implications than previous work. The first is the sample selection: rather than identifying candidate stripped nuclei by mass or size, it is done here by dynamical M/L_V, and the two subsamples have similar stellar masses and sizes (excepting a few outliers). The dynamical selection of the candidate stripped nuclei should enhance the purity of the sample, and the rate of dynamically formed X-ray binaries ought not be too dissimilar between the subsamples, allowing a direct comparison between them.

The other difference compared to past papers is the use of deep X-ray data for a relatively nearby galaxy. The median X-ray upper limit of 5×10^{36} erg s^{-1} is more than an order of magnitude deeper than in the study of Pandya et al. (2016). This is why we see a much higher X-ray detection rate (23% for the high-M/L_V subset and 33% for the full sample) than the 3% detection rate reported by that previous paper. It also means that we can reach Eddington ratios expected for low-luminosity active galactic nuclei, such that the X-ray limits are constraining at the expected black hole masses.

Despite these much deeper X-ray limits, we still find no evidence for an excess of X-ray sources in candidate stripped nuclei. If the elevated M/L_V observed in these objects is indeed due to massive black holes in many or most cases, then they must be typically accreting at $L_{bol}/L_{edd} < 2 \times 10^{-6}$. The recently discovered intermediate-mass black hole in the stripped nucleus ω Cen is remarkably faint ($L_{bol}/L_{edd} \lesssim 10^{-12}$; Häberle et al. 2024), and there is some evidence that central black holes in some nearby low-mass early-type galaxies may also have relatively low Eddington fractions (Urquhart et al. 2022). Together these observations represent emerging evidence that massive black holes in stripped nuclei—and perhaps also at the centers of low-mass galaxies that are not actively forming stars—accrete at low rates that will make them difficult to discover and characterize using X-ray or radio observations.

To take the next step will require more precise dynamical measurements of the suspected central black holes in many of these objects, which will allow their confirmation and improved constraints on their accretion properties. Unfortunately, such measurements are challenging with currently available instrumentation (Voggel et al. 2018), and accumulating a sufficient sample of precise measurements may require 30-m telescopes.

Support for this work was provided by the National Aeronautics and Space Administration through Chandra Award Number GO2-23061X issued by the Chandra X-ray Observatory Center, which is operated by the Smithsonian Astrophysical Observatory for and on behalf of the National Aeronautics Space Administration under contract NAS8-03060. We acknowledge support from NASA grant 80NSSC21K0628. This work was supported by the NSF REU program, NSF Division of Physics, Award No. 2050733. We acknowledge support from the Packard Foundation.

This research has made use of data obtained from the Chandra Data Archive and the Chandra Source Catalog, both provided by the Chandra X-ray Center (CXC).

Based on observations obtained with XMM-Newton, an ESA science mission with instruments and contributions directly funded by ESA Member States and NASA.

Table 1. X-Ray Properties of Target Sources

ID	R.A.	Decl.	M_V	M/L$_V$	Flux	X-Ray Lum.	BH Mass	Edd. Fract.	Exp. Time	Instr.
	Degrees	Degrees		$M_\odot/L_\odot$	10^{-15} ergs/s	10^{36} ergs/s	10^5 $M_\odot$	10^{-6}	ksec	
HGHH92-C23	201.477417	−42.990389	−11.66	$1.79^{+0.14}_{-0.13}$	$72.1^{+4.0}_{-4.1}$	$126.0^{+7.0}_{-7.2}$	···	···	634	ACIS-I
HGHH-07	201.522474	−42.942327	−11.09	$2.22^{+0.07}_{-0.07}$	$8.5^{+1.6}_{-1.6}$	$14.8^{+2.7}_{-2.7}$	···	···	312	ACIS-I
HHH86-30	201.226440	−42.890201	−11.02	$1.54^{+0.82}_{-0.61}$	< 3.9	< 6.8	···	···	···	ACIS
HH-10	201.379309	−42.837526	−10.98	$2.66^{+0.71}_{-0.61}$	< 3.7	< 6.4	$3.2^{+6.6}_{-1.7}$	< 1.9	···	ACIS
K-029	201.288256	−42.983105	−10.89	$1.38^{+0.25}_{-0.22}$	$44.9^{+3.6}_{-3.7}$	$78.5^{+6.2}_{-6.5}$	···	···	634	ACIS-I
VHH81-01	200.934030	−43.186620	−10.80	$7.17^{+1.14}_{-1.08}$	< 3.3	< 5.7	$8.6^{+10.0}_{-0.1}$	< 0.6	···	XMM
VHH81-03	201.242499	−42.936124	−10.65	$1.32^{+0.21}_{-0.19}$	$4.3^{+1.2}_{-1.2}$	$7.5^{+2.0}_{-2.0}$	···	···	94	ACIS-I
vhh81-5	201.317123	−42.882801	−10.63	$2.55^{+0.43}_{-0.40}$	< 2.9	< 5.1	$2.0^{+4.1}_{-0.5}$	< 2.5	···	ACIS
HGHH92-C17	201.415542	−42.933111	−10.63	$3.61^{+0.64}_{-0.58}$	< 0.8	< 1.4	···	···	···	ACIS
KV19-442	202.432394	−42.391404	−10.55	$1.57^{+0.31}_{-0.28}$	< 5.8	< 10	···	···	···	ACIS-S

Table 1 *continued*

Table 1 *(continued)*

ID	R.A.	Decl.	M_V	M/L$_V$	Flux	X-Ray Lum.	BH Mass	Edd. Fract.	Exp. Time	Instr.
	Degrees	Degrees		$M_\odot/L_\odot$	10^{-15} ergs/s	10^{36} ergs/s	10^5 $M_\odot$	10^{-6}	ksec	
K-034	201.292745	−42.892504	−10.53	$1.21^{+0.47}_{-0.39}$	77^{+10}_{-10}	134^{+17}_{-18}	···	···	223	ACIS-I
KV19-271	201.296298	−43.509212	−10.41	$2.65^{+0.39}_{-0.38}$	< 5.0	< 8.7	$4.5^{+2.8}_{-1.4}$	< 1.9	···	ACIS-I
HGHH92-C21	201.469750	−43.096222	−10.39	$4.62^{+0.48}_{-0.47}$	$21.5^{+2.9}_{-3.0}$	$37.5^{+5.1}_{-5.4}$	···	···	598	ACIS-I
HHH86-14	201.293668	−42.747977	−10.39	$1.81^{+0.79}_{-0.49}$	< 13	< 22	···	···	···	ACIS
KV19-289	201.380317	−43.046136	−10.37	$1.87^{+0.68}_{-0.56}$	< 1.1	< 1.9	···	···	···	ACIS
HGHH-11	201.227938	−43.022712	−10.35	$5.68^{+0.80}_{-0.75}$	< 1.2	< 2.0	···	···	···	ACIS
HGHH-12	201.273697	−43.175240	−10.35	$1.49^{+0.23}_{-0.22}$	$8.0^{+2.3}_{-2.2}$	$14.0^{+4.0}_{-3.8}$	···	···	322	ACIS-I
KV19-212	200.790847	−43.874458	−10.33	$2.73^{+0.39}_{-0.39}$	< 6.4	< 11	$3.5^{+2.8}_{-0.9}$	< 3.1	···	ACIS-S
T17-1412	201.281782	−43.020912	−10.30	$1.85^{+0.26}_{-0.25}$	186^{+9}_{-9}	325^{+16}_{-16}	···	···	634	ACIS-I
HGHH-35	201.434161	−42.983166	−10.30	$1.36^{+0.34}_{-0.27}$	< 1.2	< 2.1	···	···	···	ACIS
HCH99 21	201.394375	−43.057694	−10.28	$0.68^{+0.34}_{-0.27}$	< 0.9	< 1.6	···	···	···	ACIS
H12_78	201.672201	−42.703936	−10.25	$2.82^{+0.39}_{-0.39}$	< 4.9	< 8.6	$4.6^{+2.4}_{-1.2}$	< 1.8	···	ACIS
HHH86-29	201.168230	−43.301482	−10.25	$2.46^{+0.39}_{-0.36}$	< 6.4	< 11	$1.6^{+3.7}_{-0.4}$	< 6.7	···	ACIS-S
HH-22	201.089178	−43.043633	−10.18	$1.25^{+0.44}_{-0.36}$	85^{+13}_{-13}	149^{+23}_{-23}	···	···	5	ACIS-I
HHH86-26	201.563543	−42.808168	−10.12	$1.22^{+0.34}_{-0.30}$	< 6.3	< 11	···	···	···	ACIS
HGHH92-C22	201.473208	−42.985444	−10.11	$2.88^{+0.18}_{-0.17}$	< 1.3	< 2.2	···	···	···	ACIS
HGHH-G342	201.274196	−42.983493	−10.07	$1.30^{+0.42}_{-0.35}$	< 0.9	< 1.5	···	···	···	ACIS
T17-1511	201.327091	−43.021130	−10.06	$2.45^{+0.81}_{-0.69}$	$15.9^{+2.4}_{-2.4}$	$27.8^{+4.2}_{-4.3}$	$2.4^{+3.4}_{-1.7}$	10^{+10}_{-7}	634	ACIS-I
HGHH-19	201.430768	−43.123036	−10.06	$1.24^{+0.37}_{-0.31}$	< 1.6	< 2.8	···	···	···	ACIS
R261	201.303750	−43.133083	−10.06	$1.06^{+0.27}_{-0.24}$	< 1.1	< 2.0	···	···	···	ACIS
H12_95	201.500890	−43.475899	−10.05	$1.88^{+0.29}_{-0.27}$	< 6.1	< 11	···	···	···	XMM
KV19-288	201.369036	−42.941958	−10.02	$2.72^{+0.74}_{-0.63}$	< 0.8	< 1.4	$1.9^{+2.8}_{-0.7}$	< 0.7	···	ACIS
aat329848	201.505241	−43.570995	−9.95	$1.96^{+0.29}_{-0.29}$	< 6.2	< 11	···	···	···	ACIS-I
WHH-17	201.371848	−42.963098	−9.95	$1.90^{+0.44}_{-0.39}$	$2.4^{+0.7}_{-0.7}$	$4.2^{+1.2}_{-1.2}$	···	···	186	ACIS-I
H12_106	201.386037	−43.560646	−9.93	$1.88^{+1.13}_{-0.85}$	< 6.2	< 11	···	···	···	ACIS-I
pff_gc-098	201.724630	−43.321592	−9.92	$1.79^{+0.26}_{-0.26}$	< 3.3	< 5.7	···	···	···	XMM
HHH86-36	201.532145	−42.866721	−9.91	$2.21^{+0.74}_{-0.61}$	$5.2^{+1.0}_{-1.0}$	$9.0^{+1.8}_{-1.8}$	···	···	127	ACIS-I
pff_gc-100	201.764180	−42.454757	−9.86	$1.38^{+0.48}_{-0.38}$	< 7.7	< 13	···	···	···	XMM
HGHH-G204	201.445728	−43.034851	−9.85	$2.62^{+0.54}_{-0.48}$	< 0.8	< 1.5	$1.9^{+1.9}_{-0.8}$	< 0.7	···	ACIS
HHH86-34	201.419139	−43.353852	−9.85	$2.19^{+0.83}_{-0.68}$	225^{+16}_{-17}	393^{+28}_{-30}	···	···	40*	XMM
WHH-22	201.397118	−43.091414	−9.83	$1.11^{+0.44}_{-0.35}$	$1.9^{+0.3}_{-0.4}$	$3.4^{+0.6}_{-0.7}$	···	···	634	ACIS-I
HHH86-37	201.544021	−42.895178	−9.83	$1.13^{+0.33}_{-0.28}$	$7.7^{+1.9}_{-2.0}$	$13.5^{+3.3}_{-3.5}$	···	···	349	ACIS-I
WHH-18	201.375285	−42.946367	−9.78	$1.83^{+0.49}_{-0.51}$	< 0.8	< 1.5	···	···	···	ACIS
HHH86-28	201.075206	−42.816956	−9.75	$1.98^{+0.54}_{-0.43}$	< 5.9	< 10	···	···	···	ACIS
HHH86-38	201.599020	−42.900292	−9.72	$1.60^{+0.31}_{-0.27}$	< 2.5	< 4.3	···	···	···	ACIS
HHH86-33	201.317717	−42.848127	−9.68	$0.87^{+0.34}_{-0.27}$	< 3.9	< 6.7	···	···	···	ACIS
Fluffy	199.545360	−44.157251	−9.67	$2.99^{+0.85}_{-0.71}$	< 5.9	< 10	$0.8^{+2.1}_{-0.3}$	< 13	···	ACIS-S
KV19-280	201.334631	−42.985827	−9.66	$2.47^{+0.50}_{-0.44}$	< 1.2	< 2.1	$1.9^{+1.4}_{-0.8}$	< 1.1	···	ACIS
KV19-273	201.304097	−42.989558	−9.59	$3.12^{+0.96}_{-0.79}$	< 0.9	< 1.5	$2.0^{+2.3}_{-1.0}$	< 0.7	···	ACIS
HGHH-43	201.269935	−43.160808	−9.57	$0.91^{+0.32}_{-0.27}$	< 2.7	< 4.8	···	···	···	ACIS
PFF-gc056	201.386638	−42.940098	−9.52	$1.53^{+0.42}_{-0.35}$	$10.1^{+2.1}_{-2.2}$	$17.6^{+3.7}_{-3.9}$	···	···	634	ACIS-I
HGHH-44	201.382221	−43.322982	−9.52	$2.23^{+0.35}_{-0.34}$	< 5.2	< 9.1	···	···	···	XMM
HGHH-G066	201.263148	−43.050712	−9.49	$1.82^{+0.57}_{-0.47}$	< 0.9	< 1.6	···	···	···	ACIS
R223	201.386667	−43.117278	−9.49	$2.04^{+0.67}_{-0.55}$	< 1.1	< 2.0	···	···	···	ACIS
HGHH-G219	201.322045	−42.979623	−9.42	$2.79^{+0.69}_{-0.58}$	< 1.2	< 2.1	$1.8^{+1.5}_{-0.8}$	< 1.1	···	ACIS
PFF-gc028	201.254757	−42.947666	−9.40	$1.15^{+0.41}_{-0.34}$	< 3.1	< 5.3	···	···	···	ACIS
KV19-295	201.418464	−43.047600	−9.34	$1.61^{+0.38}_{-0.32}$	$3.1^{+0.6}_{-0.6}$	$5.4^{+1.1}_{-1.0}$	···	···	634	ACIS-I
T17-1664	201.407702	−42.941120	−9.28	$1.75^{+0.57}_{-0.46}$	< 0.8	< 1.4	···	···	···	ACIS
HGHH-G359	201.385034	−42.980587	−9.26	$2.90^{+0.57}_{-0.51}$	$26.4^{+3.0}_{-3.1}$	$46.2^{+5.3}_{-5.5}$	$2.2^{+1.0}_{-0.8}$	23^{+10}_{-8}	634	ACIS-I
HGHH-G251	201.452204	−42.961431	−9.23	$1.33^{+0.44}_{-0.35}$	$6.0^{+2.7}_{-1.9}$	$10.5^{+4.7}_{-3.3}$	···	···	251	ACIS-S

Table 1 *continued*

Table 1 *(continued)*

ID	R.A.	Decl.	M_V	M/L$_V$	Flux	X-Ray Lum.	BH Mass	Edd. Fract.	Exp. Time	Instr.
	Degrees	Degrees		$M_\odot/L_\odot$	10^{-15} ergs/s	10^{36} ergs/s	10^5 $M_\odot$	10^{-6}	ksec	
H12_194	201.824886	−42.494562	−9.10	$3.02^{+0.90}_{-0.74}$	< 5.1	< 9.0	$1.7^{+1.4}_{-0.8}$	< 5.1	···	XMM
T17-1444	201.299889	−42.953690	−9.10	$2.57^{+0.71}_{-0.61}$	$7.0^{+2.0}_{-2.2}$	$12.1^{+3.5}_{-3.9}$	$1.2^{+1.1}_{-0.7}$	9^{+8}_{-6}	315	ACIS-I
T17-1253	201.204815	−43.086707	−8.66	$2.77^{+0.89}_{-0.73}$	$1.6^{+0.7}_{-0.7}$	$2.8^{+0.1}_{-0.1}$	$1.1^{+0.9}_{-0.6}$	$2.4^{+0.9}_{-0.6}$	191	ACIS-I
H12_141	202.112521	−43.267474	−9.70	$1.25^{+0.22}_{-0.20}$	···	···	···	···	···	···
HGHH-41	201.162357	−43.335133	−9.66	$2.39^{+0.37}_{-0.35}$	···	···	$1.1^{+1.8}_{-0.4}$	···	···	···

Note—Column 1 is the Discovery ID for all 65 luminous globular clusters, largely pulled from (Dumont et al. 2022). Columns 2 and 3 are the source right ascension and declination in J2000 respectively. Column 4 is the visible magnitude of the source from (Dumont et al. 2022). Column 5 is the mass to visible light ratio calculated through integrated velocity dispersion measurements predominately from (Dumont et al. 2022). Column 6 is the 1-10 keV unabsorbed X-ray flux as either a detection or upper limit for the source. Column 7 is the 1-10 keV X-ray luminosity as either a detection or an upper limit for the source. Column 8 is a modeled black hole mass by accounting for the inflated mass to visible light ratio, modeled by (Dumont et al. 2022). Note this was only done for most of the inflated mass to visible light ratio sources. Column 9 is the Eddington fraction for a modeled black hole at the center of the cluster, assuming that all of the X-ray luminosity of the source originates from the black hole. Column 10 is the total stacked exposure time for each detected source (* for the XMM-Newton detection, the pn exposure time is quoted); note all empty rows in this column are upper limits as getting appropriate exposure times from the CSC for given coordinates is not always possible. Column 11 is the instrument used for the observation; note for Chandra observations, the Chandra Source Catalog stacks both ACIS-I and ACIS-S, so those upper limits are labeled ACIS, whereas our Chandra detections and limits are split between ACIS-I and ACIS-S.

Table 2. Spectral Fit Properties of Identified Sources

ID	Free absorption model				Fixed absorption model			
	$n_{\rm H}$	Γ	Flux	Fit Statistic / DoF	$n_{\rm H}$	Γ	Flux	Fit Statistic / DoF
HGHH92-C21	$0.23^{+0.21}_{-0.17}$	$1.2^{+0.3}_{-0.3}$	$21.5^{+2.9}_{-3.0}$	1.1(45.4/42)	[0.024]	$0.9^{+0.1}_{-0.1}$	$22.8^{+3.0}_{-3.3}$	1.2(49.7/43)
T17-1511	$0.53^{+0.30}_{-0.23}$	$2.1^{+0.5}_{-0.4}$	$15.9^{+2.4}_{-2.4}$	1.0(28.9/28)	[0.024]	$1.3^{+0.2}_{-0.2}$	$18.0^{+2.7}_{-3.0}$	1.6(45.6/29)
HGHH-G359	$0.28^{+0.18}_{-0.15}$	$1.2^{+0.3}_{-0.2}$	$26.4^{+3.0}_{-3.1}$	1.0(49.7/50)	[0.024]	$0.8^{+0.1}_{-0.1}$	$28.8^{+3.2}_{-3.4}$	1.2(59.1/51)
T17-1444*	< 0.82	$1.6^{+0.3}_{-0.3}$	$7.0^{+2.0}_{-2.2}$	0.8(106.6/132)	[0.024]	$1.6^{+0.3}_{-0.3}$	$6.8^{+2.0}_{-2.2}$	0.8(106.9/133)
HGHH92-C23	$0.18^{+0.05}_{-0.05}$	$1.7^{+0.1}_{-0.1}$	$72.1^{+4.0}_{-4.1}$	1.1(147.9/138)	[0.024]	$1.4^{+0.1}_{-0.1}$	$75.6^{+4.1}_{-4.2}$	1.3(179.8/139)
HGHH-07*	$0.31^{+0.30}_{-0.19}$	$2.4^{+0.6}_{-0.5}$	$8.5^{+1.6}_{-1.6}$	1.0(129.7/128)	[0.024]	$1.7^{+0.2}_{-0.2}$	$8.7^{+1.0}_{-1.1}$	1.1(137.0/129)
K-029	$0.18^{+0.09}_{-0.08}$	$1.6^{+0.2}_{-0.2}$	$44.9^{+3.6}_{-3.7}$	0.9(72.8/81)	[0.024]	$1.3^{+0.1}_{-0.1}$	$47.0^{+3.7}_{-3.9}$	1.0(84.6/82)
K-034	< 0.16	$1.1^{+0.2}_{-0.2}$	77^{+10}_{-10}	0.8(29.5/39)	[0.024]	$1.1^{+0.1}_{-0.1}$	$76.9^{+9.1}_{-9.9}$	0.7(29.5/40)
HGHH-12*	< 0.46	$1.7^{+0.7}_{-0.5}$	$8.0^{+2.3}_{-2.2}$	0.9(97.2/107)	[0.024]	$1.5^{+0.3}_{-0.3}$	$8.3^{+1.5}_{-1.6}$	0.9(97.9/108)
T17-1412	$0.12^{+0.05}_{-0.04}$	$1.2^{+0.1}_{-0.1}$	186^{+9}_{-9}	0.9(160.2/179)	[0.024]	$1.1^{+0.1}_{-0.1}$	192^{+9}_{-9}	1.0(173.9/180)
HHH86-34	$0.12^{+0.03}_{-0.03}$	$1.6^{+0.1}_{-0.1}$	225^{+16}_{-17}	1.1(109.5/104)	[0.024]	$1.3^{+0.1}_{-0.1}$	246^{+16}_{-17}	1.3(140.7/105)
WHH-22*	< 0.19	$2.1^{+0.9}_{-0.4}$	$1.9^{+0.3}_{-0.4}$	0.9(103.1/113)	[0.024]	$2.2^{+0.5}_{-0.4}$	$1.9^{+0.3}_{-0.4}$	0.9(103.3/114)
HHH86-37*	$0.26^{+0.31}_{-0.19}$	$2.2^{+0.7}_{-0.5}$	$7.7^{+1.7}_{-1.7}$	0.9(121.5/136)	[0.024]	$2.2^{+0.7}_{-0.5}$	$8.3^{+2.1}_{-2.1}$	0.9(125.7/137)
PFF-gc056	< 0.72	$1.3^{+0.5}_{-0.4}$	$10.1^{+2.1}_{-2.2}$	0.8(16.5/20)	[0.024]	$1.0^{+0.2}_{-0.2}$	$11.4^{+2.1}_{-2.4}$	0.9(18.7/21)
KV19-295*	< 0.21	$1.4^{+0.6}_{-0.2}$	$3.1^{+0.6}_{-0.6}$	0.8(89.2/106)	[0.024]	$1.4^{+0.3}_{-0.3}$	$3.0^{+0.5}_{-0.5}$	0.8(89.2/107)
HGHH-G251	$0.57^{+0.44}_{-0.30}$	$3.5^{+1.4}_{-0.9}$	$6.0^{+2.7}_{-1.9}$	1.8(28.7/16)	[0.024]	$1.3^{+0.3}_{-0.3}$	$5.4^{+0.9}_{-1.1}$	2.4(40.6/17)

Note—Best-fitting spectral properties of sources with sufficiently-high counts from Table 1. Column 1 is the Discovery ID for all 16 X-ray detected sources with spectral fits. Column 2 is the hydrogen column density in units of 10^{22} cm^{-2}. Column 3 is the photon index of the power-law component. Column 4 is the unabsorbed $1-10$ keV flux of the source (in units of 10^{-15} erg cm^{-2} s^{-1}). Columns 6-9 are the same as columns 2-5, but for a spectral fit that fixes the absorption to the line of sight column density ($n_{\rm H} = 0.024 \times 10^{22}$ cm^{-2}).

*Source fit with Cash statistics.

REFERENCES

Afanasiev, A. V., Chilingarian, I. V., Mieske, S., et al. 2018, Monthly Notices of the Royal Astronomical Society, 477, 4856, doi: 10.1093/mnras/sty913

Ahn, C. P., Seth, A. C., den Brok, M., et al. 2017, The Astrophysical Journal, 839, 72, doi: 10.3847/1538-4357/aa6972

Ahn, C. P., Seth, A. C., Cappellari, M., et al. 2018, The Astrophysical Journal, 858, 102, doi: 10.3847/1538-4357/aabc57

Arnaud, K. A. 1996, in Astronomical Society of the Pacific Conference Series, Vol. 101, Astronomical Data Analysis Software and Systems V, ed. G. H. Jacoby & J. Barnes, 17

Brodie, J. P., Romanowsky, A. J., Strader, J., & Forbes, D. A. 2011, AJ, 142, 199, doi: 10.1088/0004-6256/142/6/199

Cash, W. 1979, ApJ, 228, 939, doi: 10.1086/156922

Dabringhausen, J., Kroupa, P., Pflamm-Altenburg, J., & Mieske, S. 2012, The Astrophysical Journal, 747, 72, doi: 10.1088/0004-637X/747/1/72

Drinkwater, M. J., Gregg, M. D., Hilker, M., et al. 2003, Nature, 423, 519, doi: 10.1038/nature01666

Drinkwater, M. J., Jones, J. B., Gregg, M. D., & Phillipps, S. 2000, Publications of the Astronomical Society of Australia, 17, 227, doi: 10.1071/AS00034

Dumont, A., Seth, A. C., Strader, J., et al. 2022, ApJ, 929, 147, doi: 10.3847/1538-4357/ac551c

Evans, I. N., Primini, F. A., Glotfelty, K. J., et al. 2010, ApJS, 189, 37, doi: 10.1088/0067-0049/189/1/37

Evstigneeva, E. A., Gregg, M. D., Drinkwater, M. J., & Hilker, M. 2007, The Astronomical Journal, 133, 1722, doi: 10.1086/511958

Fruscione, A., McDowell, J. C., Allen, G. E., et al. 2006, in Society of Photo-Optical Instrumentation Engineers (SPIE) Conference Series, Vol. 6270, Observatory Operations: Strategies, Processes, and Systems, ed. D. R. Silva & R. E. Doxsey, 62701V, doi: 10.1117/12.671760

Häberle, M., Neumayer, N., Seth, A., et al. 2024, Nature, 631, 285, doi: 10.1038/s41586-024-07511-z

Haşegan, M., Jordán, A., Côté, P., et al. 2005, The Astrophysical Journal, 627, 203, doi: 10.1086/430342

Harris, G. L. H., Rejkuba, M., & Harris, W. E. 2010, PASA, 27, 457, doi: 10.1071/AS09061

Harris, W. E., Harris, G. L. H., Holland, S. T., & McLaughlin, D. E. 2002, The Astronomical Journal, 124, 1435, doi: 10.1086/342017

HI4PI Collaboration, Ben Bekhti, N., Flöer, L., et al. 2016, A&A, 594, A116, doi: 10.1051/0004-6361/201629178

Hilker, M., Infante, L., Vieira, G., Kissler-Patig, M., & Richtler, T. 1999, Astronomy and Astrophysics Supplement Series, 134, 75, doi: 10.1051/aas:1999434

Ho, L. C. 2009, The Astrophysical Journal, 699, 626, doi: 10.1088/0004-637X/699/1/626

Hou, M., & Li, Z. 2016, ApJ, 819, 164, doi: 10.3847/0004-637X/819/2/164

Hughes, A. K., Sand, D. J., Seth, A., et al. 2021, ApJ, 914, 16, doi: 10.3847/1538-4357/abf63c

Ibata, R. A., Gilmore, G., & Irwin, M. J. 1994, Nature, 370, 194, doi: 10.1038/370194a0

Irwin, J. A., Maksym, W. P., Sivakoff, G. R., et al. 2016, Nature, 538, 356, doi: 10.1038/nature19822

Kraft, R. P., Burrows, D. N., & Nousek, J. A. 1991, ApJ, 374, 344, doi: 10.1086/170124

Kraft, R. P., Kregenow, J. M., Forman, W. R., Jones, C., & Murray, S. S. 2001, The Astrophysical Journal, 560, 675, doi: 10.1086/323056

Lin, D., Strader, J., Carrasco, E. R., et al. 2018, Nature Astronomy, 2, 656, doi: 10.1038/s41550-018-0493-1

Lin, D., Strader, J., Romanowsky, A. J., et al. 2020, The Astrophysical Journal, 892, L25, doi: 10.3847/2041-8213/ab745b

Maccarone, T. J. 2004, Monthly Notices of the Royal Astronomical Society, 351, 1049, doi: 10.1111/j.1365-2966.2004.07859.x

Mieske, S., Frank, M. J., Baumgardt, H., et al. 2013, Astronomy and Astrophysics, 558, A14, doi: 10.1051/0004-6361/201322167

Minniti, D., Rejkuba, M., Funes, J. G., & Akiyama, S. 2004, The Astrophysical Journal, 600, 716, doi: 10.1086/379642

Neumayer, N., Seth, A., & Böker, T. 2020, Astronomy and Astrophysics Review, 28, 4, doi: 10.1007/s00159-020-00125-0

Pandya, V., Mulchaey, J., & Greene, J. E. 2016, The Astrophysical Journal, 819, 162, doi: 10.3847/0004-637X/819/2/162

Pechetti, R., Seth, A., Kamann, S., et al. 2022, The Astrophysical Journal, 924, 48, doi: 10.3847/1538-4357/ac339f

Pfeffer, J., Griffen, B. F., Baumgardt, H., & Hilker, M. 2014, Monthly Notices of the Royal Astronomical Society, 444, 3670, doi: 10.1093/mnras/stu1705

Phillipps, S., Drinkwater, M. J., Gregg, M. D., & Jones, J. B. 2001, The Astrophysical Journal, 560, 201, doi: 10.1086/322517

Phillipps, S., Young, A. J., Drinkwater, M. J., Gregg, M. D., & Karick, A. 2013, Monthly Notices of the Royal Astronomical Society, 433, 1444, doi: 10.1093/mnras/stt820

Ruiz, A., Georgakakis, A., Gerakakis, S., et al. 2022, MNRAS, 511, 4265, doi: 10.1093/mnras/stac272

Seth, A. C., Dalcanton, J. J., Hodge, P. W., & Debattista, V. P. 2006, The Astronomical Journal, 132, 2539, doi: 10.1086/508994

Seth, A. C., van den Bosch, R., Mieske, S., et al. 2014, Nature, 513, 398, doi: 10.1038/nature13762

Somerville, R. S., & Davé, R. 2015, Annual Review of Astronomy and Astrophysics, 53, 51, doi: 10.1146/annurev-astro-082812-140951

Soria, R., Musaeva, A., Wu, K., et al. 2017, Monthly Notices of the Royal Astronomical Society, 469, 886, doi: 10.1093/mnras/stx888

Strader, J., Seth, A. C., Forbes, D. A., et al. 2013, The Astrophysical Journal, 775, L6, doi: 10.1088/2041-8205/775/1/L6

Urquhart, R., McDermott, L. I., Strader, J., et al. 2022, The Astrophysical Journal, 940, 111, doi: 10.3847/1538-4357/ac96e6

Voggel, K. T., Seth, A. C., Baumgardt, H., et al. 2019, The Astrophysical Journal, 871, 159, doi: 10.3847/1538-4357/aaf735

Voggel, K. T., Seth, A. C., Sand, D. J., et al. 2020, ApJ, 899, 140, doi: 10.3847/1538-4357/ab6f69

Voggel, K. T., Seth, A. C., Neumayer, N., et al. 2018, The Astrophysical Journal, 858, 20, doi: 10.3847/1538-4357/aabae5

Volonteri, M. 2010, Astronomy and Astrophysics Review, 18, 279, doi: 10.1007/s00159-010-0029-x

Webb, N. A., Coriat, M., Traulsen, I., et al. 2020, A&A, 641, A136, doi: 10.1051/0004-6361/201937353

Wilms, J., Allen, A., & McCray, R. 2000, ApJ, 542, 914, doi: 10.1086/317016

Woodley, K. A., Raychaudhury, S., Kraft, R. P., et al. 2008, The Astrophysical Journal, 682, 199, doi: 10.1086/529419

Wrobel, J. M., Miller-Jones, J. C. A., & Middleton, M. J. 2016, The Astronomical Journal, 152, 22, doi: 10.3847/0004-6256/152/1/22

Wrobel, J. M., & Nyland, K. E. 2020, The Astrophysical Journal, 900, 134, doi: 10.3847/1538-4357/aba8f7

Zhang, Z., Gilfanov, M., Voss, R., et al. 2011, Astronomy and Astrophysics, 533, A33, doi: 10.1051/0004-6361/201116936